JOURNAL OF GEOPHYSICAL RESEARCH, VOL. 115, C03019, doi:10.1029/2009JC005417, 2010

Click Here for Full Article

Wind-generated eddy characteristics in the lee of the island of Hawaii

Sachiko Yoshida,[1] Bo Qiu,[2] and Peter Hacker[1]

Received 2 April 2009; revised 23 October 2009; accepted 30 October 2009; published 17 March 2010.

[1] Weekly satellite sea surface height (SSH) anomaly data are used to clarify the mesoscale eddy characteristics in the lee of the island of Hawaii, the largest island in the Hawaiian Island chain. The lee eddy variability can be separated into two geographical regions. In the immediate lee southwest of Hawaii (Region E), eddy signals have a predominant 60 day period and a short life-span, whereas in the region along 19°N west of ~160°W (Region W), the eddy variability is dominated by 100 day signals and extends over a broad region. By applying a linear Ekman pumping model forced by the weekly QuikSCAT wind data, we find that the observed 60 day eddy signals originate in the southwest corner of Hawaii and are induced by the local 60 day wind stress curl variability associated with the blocking of the trade wind by the island of Hawaii. The relationship between the wind forcing and the observed SSH signals demonstrates the role of the ocean as an integrator that responds more effectively to the low-frequency synoptic atmospheric forcing (~60 days) than to the higher-frequency forcing (~30 days). Since the large-amplitude 60 day SSH anomalies take 1–2 weeks to fully develop, it is possible that real-time observed wind stress data can be used for the prediction of these anomalies. In contrast to the wind-induced 60 day eddy signals in the lee of the island of Hawaii, the 100 day eddy signals in Region W are likely generated by the instability of the sheared North Equatorial Current and Hawaii Lee Countercurrent.

Citation: Yoshida, S., B. Qiu, and P. Hacker (2010), Wind-generated eddy characteristics in the lee of the island of Hawaii, *J. Geophys. Res.*, *115*, C03019, doi:10.1029/2009JC005417.

1. Introduction

[2] Located at the center of the North Pacific subtropical gyre, the Hawaiian archipelago is considered to be a key region for generating mesoscale eddies for the western Pacific Ocean. Recent advances in the observation network enable us to see unique features of both the atmospheric and oceanic circulations within this region. Figure 1 shows the drifter-derived mean velocity of *Maximenko et al.* [2008]. The large-scale surface currents indicate the eastward flowing North Pacific Subtropical Countercurrent (STCC) [*Uda and Hasunuma*, 1969; *Hasunuma and Yoshida*, 1978] north of 24°N and the westward flowing North Equatorial Current (NEC) to the south. The NEC bifurcates at the island of Hawaii (also known as the Big Island) around (20°N, 155°W), and its northern part flows northwestward along the Hawaiian ridge as the North Hawaiian Ridge Current (NHRC) [*Firing*, 1996; *Firing et al.*, 1999]. An important narrow eastward flow called the Hawaiian Lee Countercurrent (HLCC) along 19.5°N was found in late 1990s by the analysis of surface drifter data [*Qiu et al.*, 1997]. As the HLCC approaches the island of Hawaii, the current separates into two branches. The northern branch continues along the island chain and becomes the northwestward flowing Hawaiian Lee Current (HLC) [*Lumpkin*, 1998], and the southern branch merges into the westward flowing NEC. With the HLC to the north and the NEC to the south, there exists a strong north-south horizontal shear centered on the HLCC, and this unique zonal flow system makes the lee region of the Hawaiian Islands abundant with cyclonic and anticyclonic eddies.

[3] From the atmospheric circulation point of view, the northeasterly trade wind throughout the year is obstructed by the volcanic high mountains, and this generates positive and negative wind stress curl anomalies on the western side of each island (see Figure 2). The wind stress curl anomaly produced by the islands of Maui and Hawaii has been shown using both observational analysis and numerical modeling to be the major cause for driving the HLCC [*Xie et al.*, 2001; *Sakamoto et al.*, 2004]. In addition, the warm water advection by the eastward HLCC gives rise to a coupled ocean–atmosphere response observable as a wake extending over a great distance to the west of the Hawaiian Islands [*Xie et al.*, 2001; *Sasaki and Nonaka*, 2006].

[4] The combination of the ocean and atmosphere circulation systems makes the region to the west of the island of Hawaii more energetic in mesoscale eddy variability than the surrounding areas, and the high eddy activity is closely

[1]International Pacific Research Center, University of Hawai'i at Mānoa, Honolulu, Hawaii, USA.
[2]Department of Oceanography, University of Hawai'i at Mānoa, Honolulu, Hawaii, USA.

Copyright 2010 by the American Geophysical Union.
0148-0227/10/2009JC005417

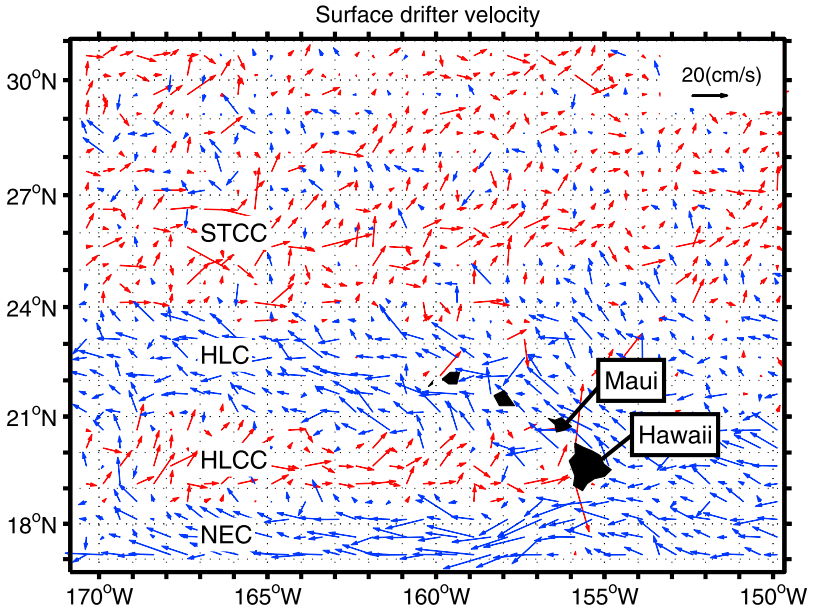

Figure 1. Ensemble-mean drifter velocity calculated from the data of the Atlantic Oceanographic and Meteorological Laboratory (NOAA), Miami, Florida [*Maximenko et al.*, 2008]. Velocity vectors with eastward and westward components are plotted in red and blue, respectively. HLC, Hawaiian Lee Current; HLCC, Hawaiian Lee Countercurrent; NEC, North Equatorial Current (NEC); STCC, North Pacific Subtropical Countercurrent.

related to the regional dipole-structured wind stress curl anomalies. Using numerical simulations, *Calil et al.* [2008] showed that the oceanic variability in the lee of the Hawaiian Islands is sensitive to the temporal and spatial resolutions of the regional surface wind forcing. Enhanced oceanic eddy variability due to regional, orographic wind forcing is not unique to the lee of the Hawaiian Islands. In the gulfs of Tehuantepec and Papagayo in the eastern tropical Pacific Ocean, isolated mesoscale eddies off the Central American coast have been shown to be induced by strong, intermittent, offshore winds during the boreal cold season [*Clarke*, 1998; *McCreary et al.*, 1989; *Lavín et al.*, 1992; *Giese et al.*, 1994; *Trasviña et al.*, 1995; *Müller-Karger and Fuentes-Yaco*, 2000]. On interannual time scales, generation of Tehuantepec eddy signals has been further shown to be modulated by incoming coastally trapped waves associated with the El Niño and La Niña events [e.g., *Zamudio et al.*, 2006].

[5] Around the Hawaiian archipelago, the observed sea surface height (SSH) anomalies show two high-eddy-variability regions: one is north of the island chain centered along 26°N, and the other is in the lee of the island of Hawaii along ~20°N (Figure 3a). These two high-variability regions are located over the broad and narrow eastward flows of the STCC and the HLCC, respectively. The variability is generated not only by the wind forcing, but also by the oceanic instabilities due to horizontal and vertical current shears [*Qiu*, 1999]. For the seasonal eddy variation,

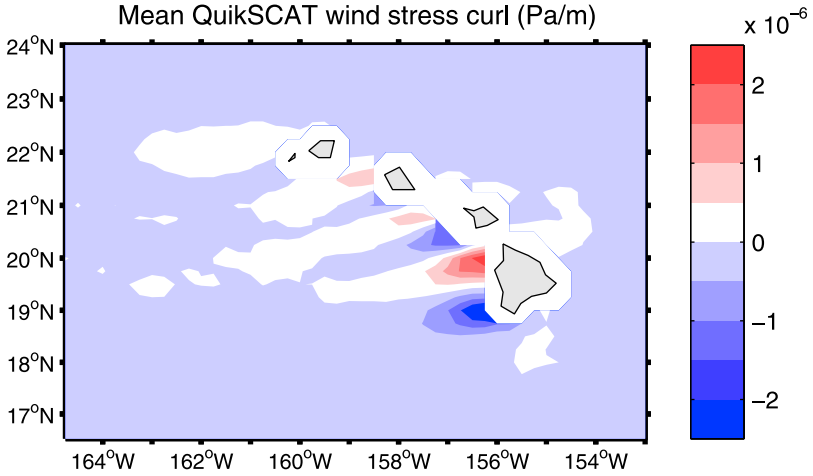

Figure 2. Mean QuikSCAT wind stress curl distribution over the period 1999–2008.

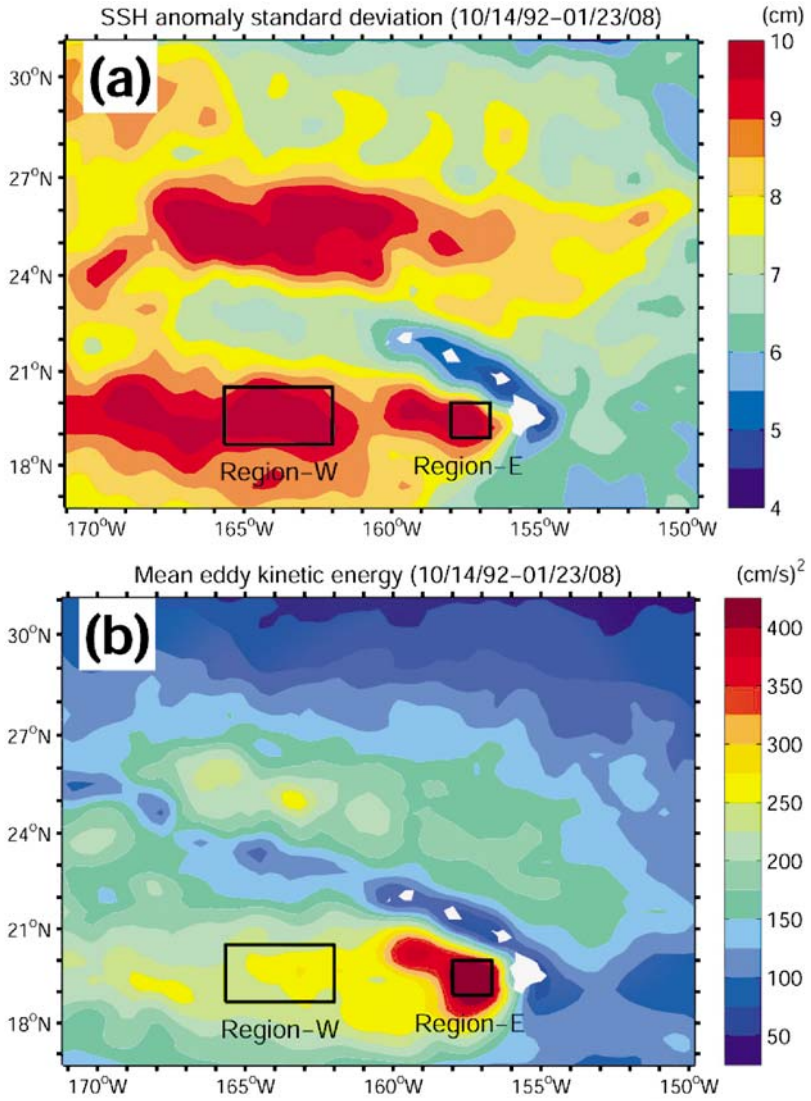

Figure 3. (a) Root mean square sea surface height (SSH) anomaly (SSHA) and (b) mean eddy kinetic energy around the Hawaiian Islands calculated from Archiving, Validation, and Interpretation of Satellite Oceanographic merged satellite data.

Kobashi and Kawamura [2002] pointed out that the HLCC becomes baroclinically more unstable during late fall to winter as a result of a stronger vertical velocity shear and a weaker stratification between the HLCC and the subsurface westward flow. In addition to the physical processes, lee eddy activity is also important for the regional biological productivity [*Nencioli et al.*, 2008; *Kuwahara et al.*, 2008; *Dickey et al.*, 2008].

[6] In the lee of the island of Hawaii, satellite SSH anomaly data have been used to explore the origin and pathways of mesoscale eddies. Eddies formed in the lee of the island of Hawaii are known to travel for long distances. For example, *Mitchum* [1995] found 90 day signals from the tide gauge record at Wake Island and indicated that the origin of the observed oscillations started from the lee of the island of Hawaii. By focusing on individual eddies, *Holland and Mitchum* [2001] explored the eddy paths and propagation characteristics on the basis of satellite data analysis and discussed the interaction of mesoscale eddies with the zonal flow of the NEC. Generation of the Hawaii lee eddies has been hypothesized as being due to the NEC's impinging upon the Hawaiian Islands through the mechanism of Karman vortex street [*Lamb*, 1945]. It is important to note that a stable Karman vortex street is observable only when oppositely signed eddies are generated alternately on the two tips of an island. With the constricted Alenuihaha Channel between Maui and Hawaii, generation of cyclonic eddies at the northwestern tip of the island of Hawaii is rare. Indeed, satellite SSH data to be presented in this study reveal that both positive and negative SSH eddy signals are generated southwest of the island of Hawaii. These observational results imply that the Karman vortex street is not a viable eddy generation mechanism for the lee of Hawaii.

[7] Our present study has two objectives. The first objective is to clarify the lee eddy characteristics through the analysis of satellite altimeter data. We categorize the lee

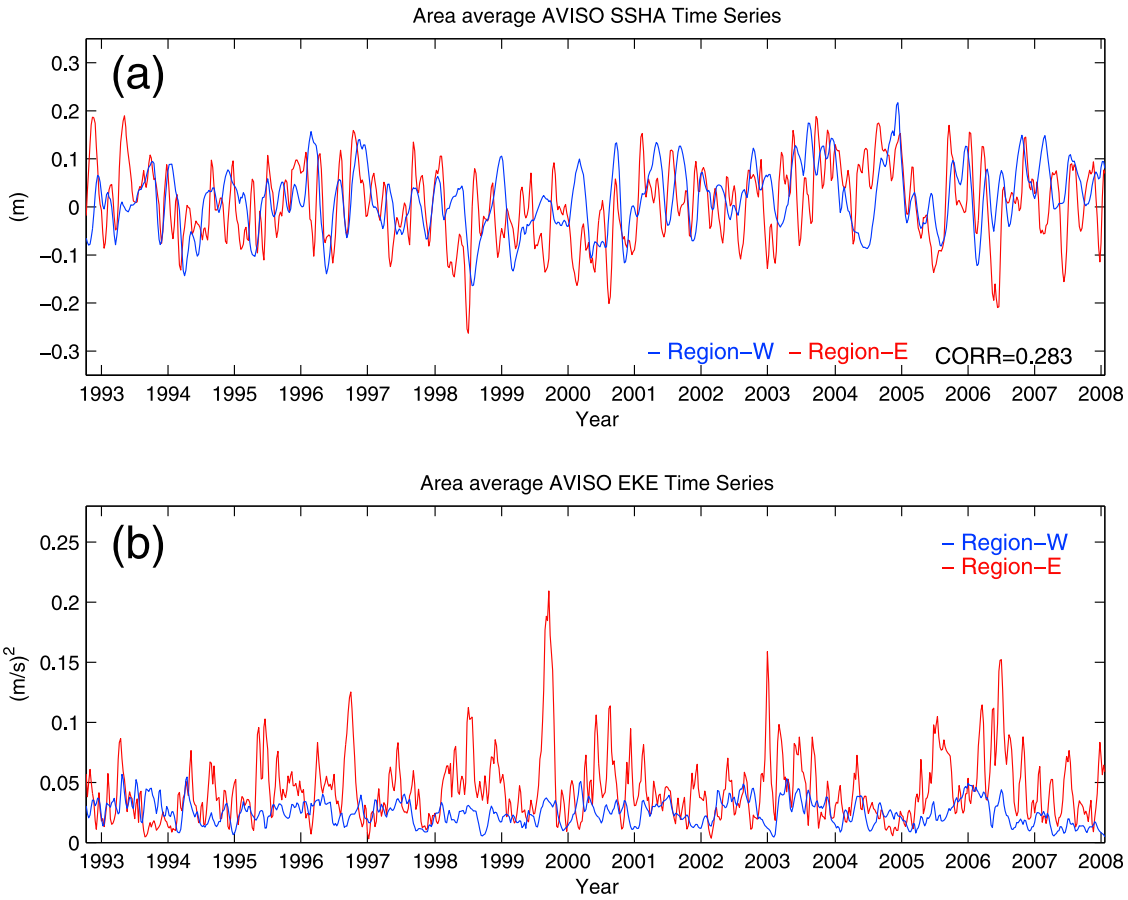

Figure 4. (a) SSHA and (b) eddy kinetic energy (EKE) time series at two locations along 19.5°N calculated from altimetric SSH anomaly data. Blue and red curves represent variability at Region W and Region E, respectively. AVISO, Archiving, Validation, and Interpretation of Satellite Oceanographic data.

eddy signals based on their temporal and spatial scales in order to better understand the strong SSH variability over the relatively large area in the lee region, including the 90 day signal discussed by *Mitchum* [1995]. The second objective is to quantify the effect of wind forcing in inducing the lee eddy variability. As reviewed above, Hawaii lee eddies can be formed by both wind forcing and barotropic and/or baroclinic instabilities of the background mean flow. The relative importance of these forcing mechanisms depends on the signals in the specific regions of interest. For example, it is possible that the wind forcing has a greater impact upon the variability in the immediate lee region than in the upstream region of the HLCC. Although it has been argued that the anomalous wind forcing is important to the SSH signals in the lee of the Hawaiian Islands, a clear relationship between the wind forcing and the surface variability is yet to be established. Specifically, there remain questions such as how much of the SSH anomalies is directly caused by the wind forcing, where the eddy is formed, how far the eddy can travel, and if and where the eddy path terminates in the lee of the island of Hawaii.

[8] The paper is organized as follows. Mesoscale eddy features are first discussed using the spatial and temporal distributions of the observed SSH variability and eddy kinetic energy (EKE) fields in section 2. The relationship between the lee eddy and the wind forcing is explored in section 3 on the basis of the QuikSCAT wind stress forcing analysis and a simple Ekman pumping model applied to the immediate lee region. In section 4, details about the formation and propagation of the wind-induced eddy signals are investigated through a composite analysis. We summarize the results in section 5.

2. Sea Level Variability Characteristic Over the Hawaiian Lee Countercurrent

[9] For this study, we use the global SSH anomaly data set provided by the Collecte Localisation Satellites Space Oceanographic Division of Toulouse, France (http://www.aviso.oceanobs.com/). This is a merged data set with TOPEX/Poseidon, European Remote Sensing Satellite, Geosat Follow-On, and Jason 1 along-track SSH measurements. It covers the period from October 1992 to January 2008 with a weekly interval and a 1/3° × 1/3° spatial resolution.

[10] Using more than 15 years of the altimetric data, we plot the root mean square (RMS) SSH anomaly distribution as well as that of the eddy kinetic energy in Figure 3. The eddy kinetic energy is estimated from the gridded SSH

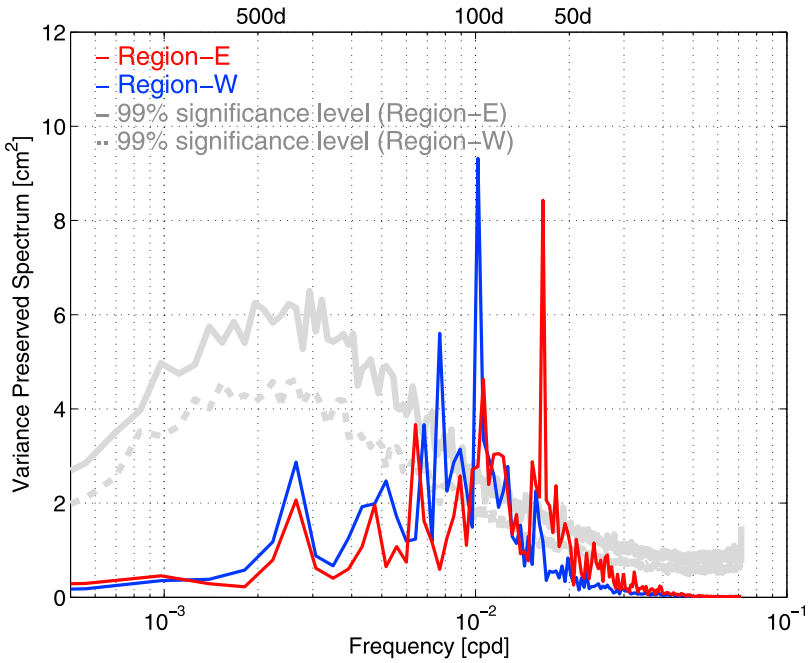

Figure 5. Power spectra of SSH anomalies in Region W (blue) and Region E (red) plotted in variance-preserving form. Shaded curves indicate 99% significance levels from the Monte Carlo simulations at Region E (solid line) and Region W (dashed line).

anomaly data by assuming geostrophy. Two distinct areas emerge with the RMS amplitude exceeding 9.5 cm over the HLCC region. One is close to the island of Hawaii around 159°W–157°W, and the other extends over a broader region around 169°W–162°W with a continuous high-variability band. In contrast, the large eddy kinetic energy is concentrated only in the immediate lee of Hawaii centered around 157°W. The mean eddy kinetic energy level in this east HLCC region exceeds 400 $(\mathrm{cm/s})^2$, and the energy level weakens to the west, with the mean eddy kinetic energy level dropping below 300 $(\mathrm{cm/s})^2$ west of 160°W. The different ratio between the RMS SSH variability and the EKE level in the east and west parts of HLCC implies that the eddy variability in these two geographical regions has different dominant spatial scales. Specifically, let the SSH anomaly variance be $\langle\hat{\eta}^2\rangle$; then

$$\mathrm{EKE} \equiv \left(k^2 + l^2\right)\langle\hat{\eta}^2\rangle\frac{g^2}{f^2}, \qquad (1)$$

where f is the Coriolis parameter, g is the gravitational constant, and k and l are horizontal wave numbers in the longitude and latitude directions, respectively. With the observed $\langle\hat{\eta}^2\rangle$ being of similar amplitudes, the high EKE level in the east HLCC region indicates that the local eddy signals have smaller spatial scales (larger k, l values) than those in the west HLCC. Since the temporal and spatial scales are commonly proportionally related, this also suggests that the temporal scales near 157°W are shorter. This is indeed the case, as will be confirmed in Figure 5.

[11] Figure 4 shows the time series of the area average SSH anomaly and eddy kinetic energy in the two regions of interest: the immediate lee region (18.9°N–20°N, 158°W–156.7°W) and the west HLCC region (18.7°N–20.5°N, 165.6°W–162°W). For brevity, we refer to these two regions hereafter as Region E and Region W, respectively (see Figure 3). For both regions, the amplitudes of SSH anomaly are in the same range of about 20 cm, and the time series are correlated at the annual and interannual time scales. A closer look at the time series reveals that the eddy temporal scale in Region E has a higher frequency, which is consistent with equation (1). Unlike the SSH anomaly time series, eddy kinetic energy calculated from the SSH anomalies in the same areas shows prominent differences between these two regions. The amplitude in Region E, shown by the red curve in Figure 4b, is nearly double that in Region W, shown by the blue curve in Figure 4b. The mean EKE values are 0.0251 and 0.0436 $(\mathrm{m/s})^2$ for Region W and Region E, respectively, and these values are consistent with the mean EKE spatial distribution (Figure 3b).

[12] To examine the dominant eddy frequency along the HLCC band, we calculate power spectra using the 15.5-year altimetric SSH anomaly time series. Figure 5 shows the area average power spectral density distributions in Region E and Region W. Mesoscale eddy variability has a predominant peak close to 60 days (the exact spectral peak is at 60.74 days) in Region E, as shown by the red curve in Figure 5. In Region W, the largest spectral peak exists close to 100 days (the exact spectral peak is at 98.19 days). The fact that the sharp SSH peak in Region E emerges at a frequency band higher than that of Region W supports our scale estimation put forth in equation (1). The 100 day signal in Region W likely corresponds to the 90 day oscillations observed in the Wake Island sea level record reported by *Mitchum* [1995].

[13] To investigate the spatial independence of these two frequency bands of variability, we extract 60 and 100 day

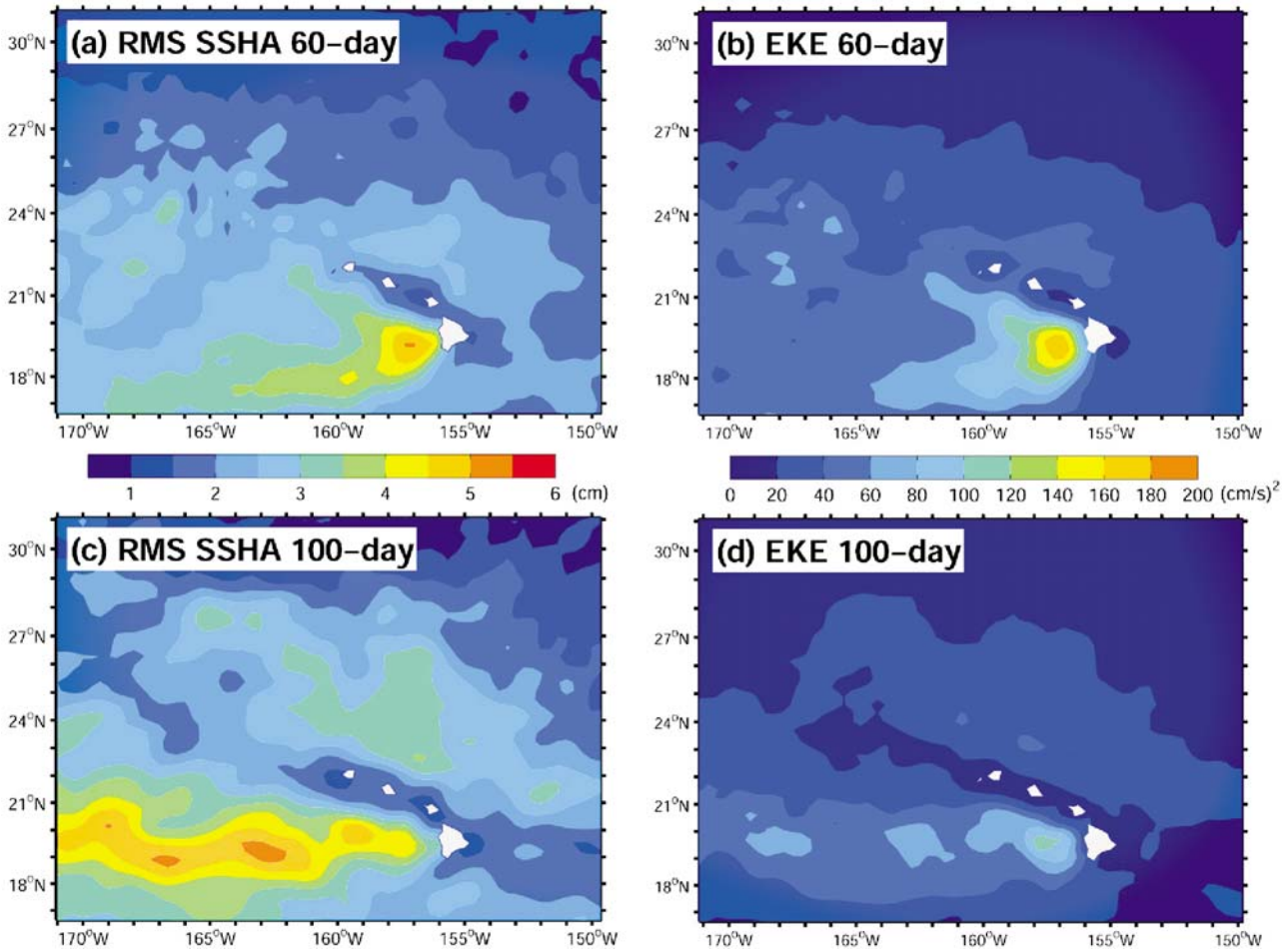

Figure 6. Horizontal maps of (a, c) the root mean square (RMS) SSH anomaly standard deviation and (b, d) EKE. The SSH anomalies were band-pass-filtered around 60 days in Figures 6a and 6b and around 100 days in Figures 6c and 6d.

signals from the original SSH anomaly time series using band-pass filters with bandwidths between 30 and 70 days and between 80 and 110 days, respectively. We plot in Figure 6 the RMS SSH anomaly and the eddy kinetic energy distributions based on the band-pass-filtered SSH anomaly time series. For the 60 day variability, similar patterns are obtained between the RMS SSH and EKE distributions: large-amplitude 60 day signals are confined to the lee of the island of Hawaii and extend northwest and southwest in a horseshoe pattern. For the 100 day variability, the RMS SSH and EKE signals exhibit different spatial patterns: while the 100 day SSH variability is largely coherent along the entire HLCC band, the 100 day EKE signals have a local maximum in Region E with an amplitude smaller than that of the 60 day EKE signals. The constancy in the 100 day SSH signals along the HLCC band likely reflects the westward wave propagation of the 100 day signals, as noted by *Mitchum* [1995].

[14] The 60 day signals in Region E were not recognized as independent of the 100 day variability in past research. In other words, compared to the 100 day signals detected along the HLCC band in Region W, less is known about the 60 day signals observed in the immediate lee of the island of Hawaii. In the following, mechanisms responsible for generating the 60 day signals in Region E are explored.

3. The 60 Day Signal Mechanism

[15] The oceanic variability in the lee of the Hawaiian Islands is intimately related to the surface wind forcing modified by the presence of the islands' high mountains. The orographic impact upon the regional wind stress curl field and its consequence on the lee circulation of the Hawaiian Islands have been discussed in several recent papers [see *Qiu and Durland*, 2002, and references therein]. The meridional sea surface temperature (SST) gradients show the warm water supply by the eastward HLCC over a surprisingly long distance, and strong interactions between SST and surface wind convergence are detected in this area [*Xie et al.*, 2001]. However, the eddy active region does not show such a far-reaching effect compared to that of SST. As discussed in the previous section, the 60 day variability is restricted to the immediate lee region. Numerical model simulations driven by different wind products show different EKE distributions in Region E, indicating that the eddy

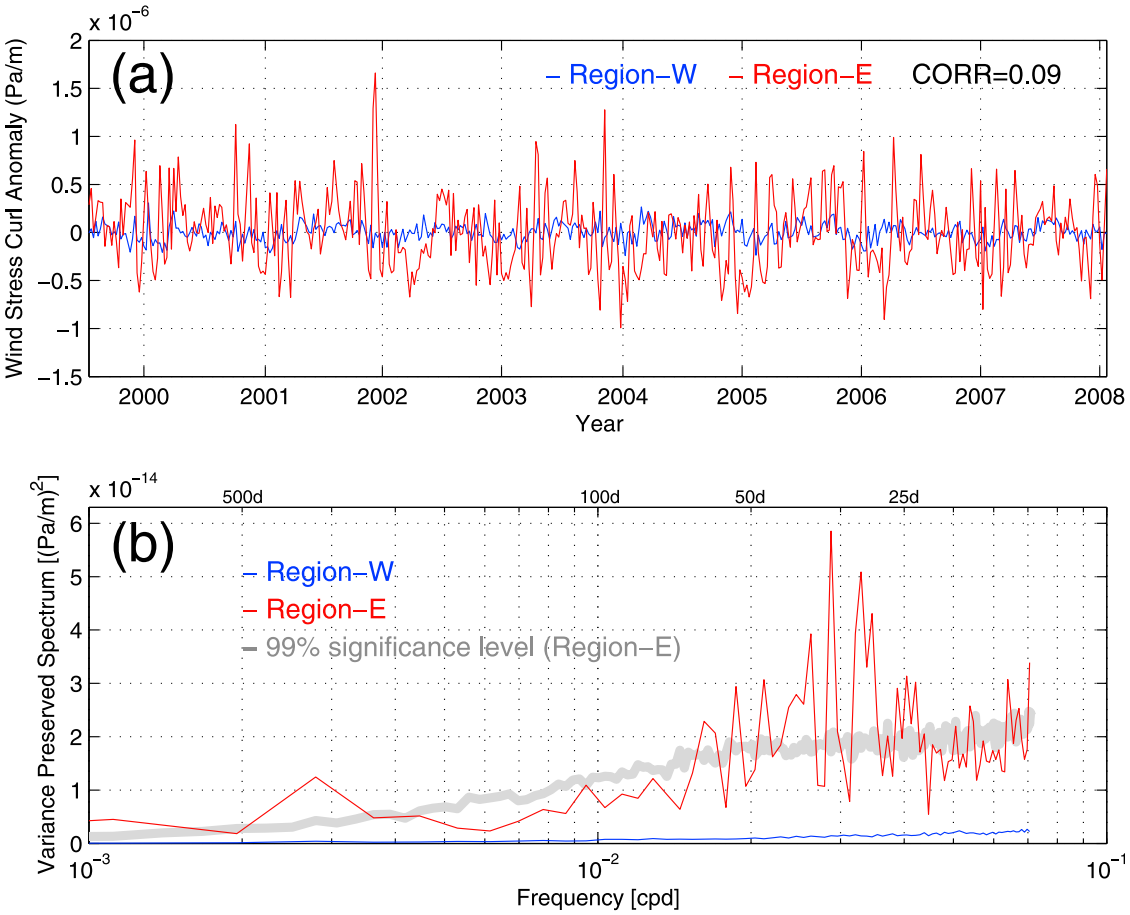

Figure 7. (a) QuikSCAT wind stress curl anomaly time series and (b) power spectra density in Region E and Region W. Gray curve in Figure 7b indicates 99% significance levels from the Monte Carlo simulations at Region E.

activity is likely controlled by the regional wind forcing [*Calil et al.*, 2008]. In this section, we examine the details of the wind stress curl data and estimate the extent to which the wind stress curl forcing explains the observed SSH anomaly data in Region E.

3.1. Wind Stress Curl Characteristics

[16] We use the gridded QuikSCAT surface wind stress product from the Asia-Pacific Data-Research Center at the University of Hawaii (http://apdrc.soest.hawaii.edu/) to investigate the relationship between the local wind stress and SSH anomalies. The data are provided with a weekly interval and a 1/4° resolution in both longitude and latitude and are available from 21 July 1999 to 23 January 2008 for 445 weeks. For this period, a few missing points are filled using a linear interpolation to get a continuous time series.

[17] Figure 2 represents the mean wind stress curl distribution calculated from the QuikSCAT data around the Hawaiian Islands. It shows the well-known pattern in which the northeasterly trade wind throughout a year sustains negative and positive pairs of wind stress curl structures in the lee of each island. Notice that the orographically induced wind stress curl forcing has a zonally elongated pattern and its influence is limited to <300 km west of the islands. As the 60 day signals are collocated with the dipolar wind stress curl forcing in the lee of the island of Hawaii, it makes sense to explore the connection between the observed SSH anomaly and those induced by the local wind forcing.

[18] To do so, we first look into whether the wind stress curl forcing in the lee of the island of Hawaii has a spectral peak close to the 60 day period. An investigation into the wind stress curl time series can also be useful in clarifying the relationship between the observed 60 versus 100 day signals. Figure 7 shows the wind stress curl time series and their power spectral density distributions in Region E and Region W. The wind stress curl time series in Region E and Region W are poorly correlated. The Region W wind stress curl has a low RMS amplitude of 0.91×10^{-7} Pa/m and contains no dominant frequencies. This implies that the local wind forcing has little influence upon the 100 day eddy signals observed in Region W. The Region E forcing, on the other hand, has energy concentrated at the monthly to intraseasonal frequency band. While the strongest spectral peaks appear near 29 and 35 days, a distinct energy peak does exist around 60 days and has a variance amplitude of 2.3×10^{-14} $(\mathrm{Pa/m})^2$ over a relatively broad width. Since the time series and the spectrum do not show a conclusive connection between the 60 day SSH variability and the wind

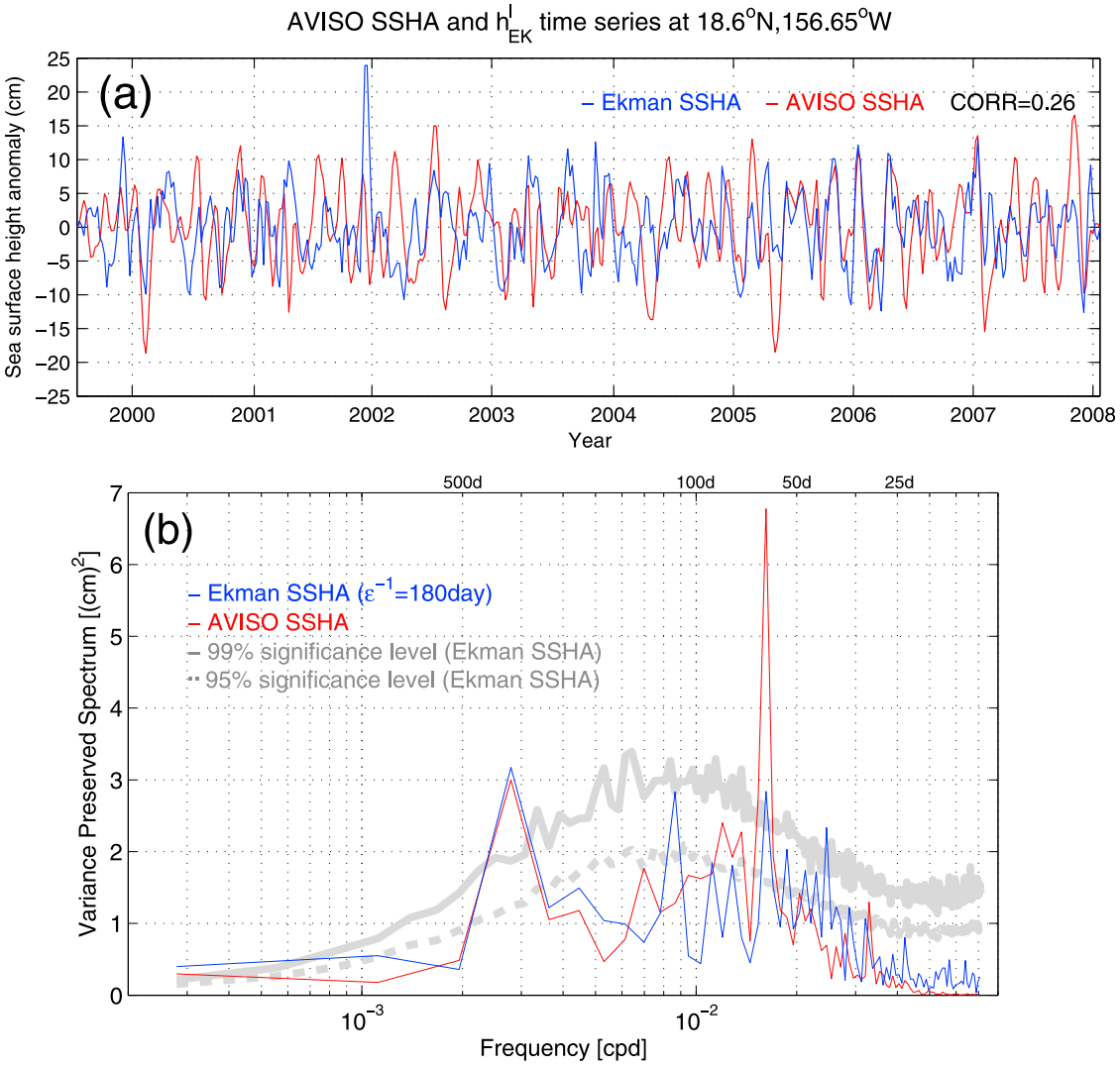

Figure 8. (a) Time series and (b) power spectral density of h'_{EK} and observed SSH anomaly at 18.6°N, 156.7°W. Solid and dashed gray curves in Figure 8b indicate 99% and 95% significance levels of the h'_{EK} SSH anomaly from the Monte Carlo simulations, respectively.

forcing, our next step is to try to adopt the linear Ekman pumping model to relate the SSH signals to the time-varying wind stress curl forcing in a quantitative way.

3.2. Linear Ekman Pumping Model

[19] The linear Ekman pumping model can be derived from the shallow-water vorticity equation [e.g., *Qiu*, 2002]. Since the domain of interest is located close to the island boundary and the 60 day variability is confined to the lee of the island, the β term in the vorticity equation can be neglected. Given that baroclinic Rossby radii of deformation in the lee of Hawaii are shorter than 60 km [e.g., *Chelton et al.*, 1998] (Figure 6), the long-wave approximation is justified. Under these conditions, the linear Ekman pumping model can be written as

$$\frac{\partial h'_{EK}}{\partial t} = -\frac{g'}{g\rho_0}\,\mathrm{curl}\left(\frac{\vec{\tau}}{f}\right) - \varepsilon h'_{EK}, \qquad (2)$$

where h'_{EK} denotes the SSH changes due to the convergence/divergence of the surface Ekman fluxes, g' is the reduced gravity (~0.03 m/s^2), ρ_0 is the reference density of seawater, and $\vec{\tau}$ is the weekly QuikSCAT wind stress vector. As the wind-induced SSH variability is subject to eddy dissipation, this process is parameterized in equation (2) by inclusion of the Newtonian damping term. For this study, we set ε = 1/180 day, and this ε value is chosen such that the eddy dissipation weakens the wind-induced, low-frequency SSH signals but has little impact upon the h'_{EK} signals with the intraseasonal frequencies that are of interest to this study.

[20] To quantify the 60 day variability in the lee of the island of Hawaii, we compare in Figure 8a the observed SSH anomaly time series at 18.6°N, 156.65°W to the h'_{EK} time series derived from equation (2). For consistency in comparison, a 180 day high-pass filter has been applied to both time series in order to remove the low-frequency signals.

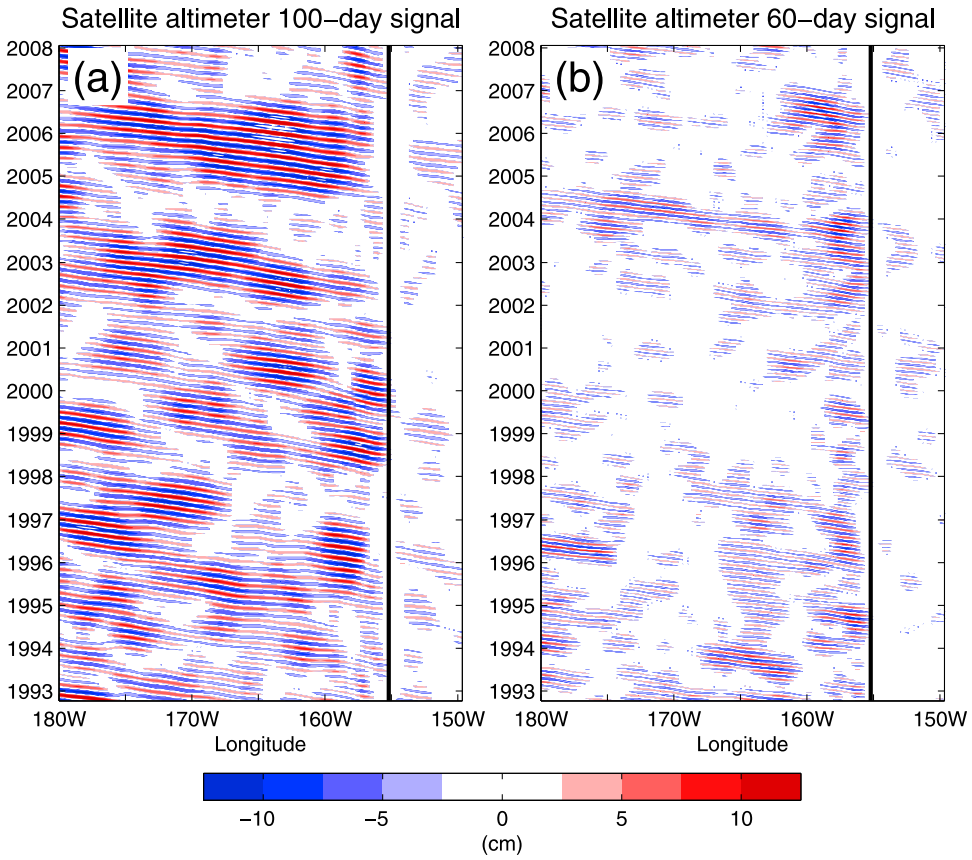

Figure 9. Longitude-time section of observed SSH anomaly band-passed around (a) 100 days and (b) 60 days along 19.5°N.

Overall, there exists a favorable correspondence between the two time series, and the h'_{EK} time series is able to capture many of the observed 60 day mesoscale eddy events, in particular after the year 2003. For signals with high frequencies, the h'_{EK} time series has larger amplitude than that of the observations. The linear correlation coefficient between the two time series shown in Figure 8a is 0.26.

[21] Figure 8b shows the power spectral density distributions of the h'_{EK} and observed SSH anomaly time series. The observed SSH anomaly has the dominant 60 day variability, with a variance amplitude of 6.77 cm^2, and the h'_{EK} time series has a relatively smaller amplitude, 2.84 cm^2, at the corresponding frequency. At the frequency band around 40–50 days, the h'_{EK} time series has a spectral amplitude comparable to that at 60 days, and the 40–50 day forcing peaks can be detected in the wind stress curl spectrum shown in Figure 7. Although the 30 day variability is most noticeable in the wind stress curl time series, its corresponding peak in the h'_{EK} spectrum in Figure 8b is hardly distinguishable.

3.3. Validation of the 60 Day Signal

[22] In order to understand why the h'_{EK} variability has a larger amplitude in the 60 day period than in the 30 day period (even though the wind stress forcing has a greater power in the latter period), it is instructive to examine the frequency-dependent SSH signals as a result of the Ekman pumping process. For simplicity, we rewrite equation (2) as

$$\frac{\partial h'_{EK}}{\partial t} = F - \varepsilon h'_{EK}, \tag{3}$$

where F denotes the convergent Ekman flux. Using the inverse Fourier transforms for $h'_{EK}(t)$ and $F(t)$,

$$h'_{EK}(t) = \frac{1}{2\pi}\int_{-\infty}^{\infty} \hat{h}(\omega) e^{i\omega t} d\omega \text{ and } F(t) = \frac{1}{2\pi}\int_{-\infty}^{\infty} \hat{F}(\omega) e^{i\omega t} d\omega,$$

we can rewrite equation (3) as

$$i\omega\hat{h}(\omega) = \hat{F}(\omega) - \varepsilon\hat{h}(\omega).$$

By multiplying the complex conjugates and rearranging, we have [*Hasselmann*, 1976]

$$|\hat{h}^2(\omega)| = |\hat{F}^2(\omega)|/(\omega^2 + \varepsilon^2). \tag{4}$$

[23] In equation (4), $|\hat{h}^2(\omega)|$ and $|\hat{F}^2(\omega)|$ are spectra for the $h'_{EK}(t)$ and $F(t)$ time series, respectively. As ω approaches zero, $|\hat{h}^2|$ approaches $|\hat{F}^2|/\varepsilon^2$, and for $\omega \gg \varepsilon$ (high-frequency signals), $|\hat{h}^2|$ approaches $|\hat{F}^2|/\varepsilon^2$. The latter result indicates that under the same strength of the forcing at different frequencies, we can expect a greater

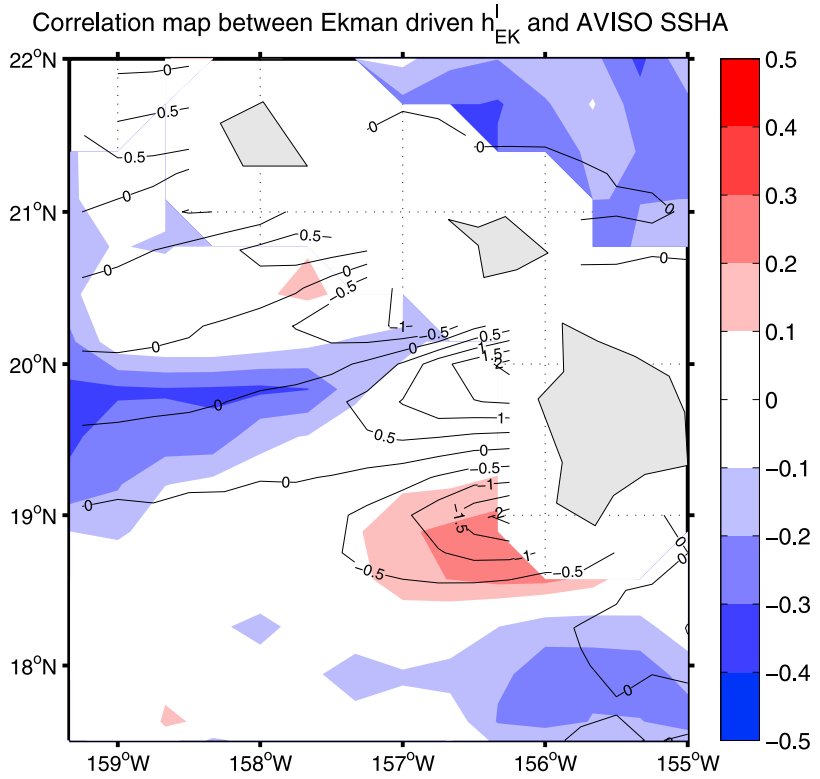

Figure 10. Correlation map between h'_{EK} and the observed SSH anomaly (color shading) and the mean wind stress curl (black contour) (values given as $\times 10^{-6}$ Pa/m).

SSH spectral power $|\hat{h}^2|$ at lower-frequency bands than at higher-frequency bands.

[24] For the high-frequency signals at 30 versus 60 days, the spectral ratio between the 30 and 60 day forcing in Figure 7 is $|\hat{F}^2_{30}|/|\hat{F}^2_{60}| \cong 2.6$. Since $\omega \gg \varepsilon$, equation (4) indicates that

$$\frac{|\hat{h}^2_{30}|}{|\hat{h}^2_{60}|} \cong \frac{\omega^2_{60}}{\omega^2_{30}} \frac{|\hat{F}^2_{30}|}{|\hat{F}^2_{60}|} = \frac{1}{4} \frac{|\hat{F}^2_{30}|}{|\hat{F}^2_{60}|} \cong 0.65.$$

This ratio corresponds well to the spectrum analysis shown in Figure 8. With the same approach, it is possible to show that the strong 50 day signal in h'_{EK} is also consistent with the surface wind stress forcing. This relationship between the wind stress curl forcing and the observed SSH signals demonstrates the role of the ocean as an integrator that responds more effectively to the lower-frequency synoptic atmospheric forcing (i.e., the 60 day forcing) than to other, higher-frequency forcing (e.g., at 30 days).

4. Wind-Induced Eddy Formation Mechanism

[25] The analysis in the previous section leads to the conclusion that the 60 day variability observed in the lee of the island of Hawaii is attributable to the local wind stress curl forcing. Figure 9 shows the longitude-time section of the observed, band-pass-filtered 100 and 60 day SSH anomalies along 19.5°N. Signals with an amplitude less than 2.5 cm are shown in white. The line at 155°W corresponds to the longitude of the island of Hawaii. It is significant that the 60 day signals are predominantly generated west of Hawaii and propagate westward with a phase speed of about 7.5 cm/s. Although some of the 60 day signals persist farther to the west (e.g., the ones formed at the end of year 2003 reach to 175°W), most of the observed 60 day signals tend to enhance the amplitude only between 158°W and 157°W and then weaken near 160°W. This could be the reason why there exists a small gap around 160°W in the SSH anomaly standard deviation distribution shown in Figure 3. Compared to the 60 day signals, the 100 day signals are continuously formed and propagate further west. The fact that the 60 day signals are mostly confined to the lee of the island of Hawaii implies that the wind-induced eddies have a relatively short life span and that they are independent of the 100 day signals in Region W discussed by *Mitchum* [1995]. Although the 60 day signals are generated continuously in the lee of Hawaii, Figure 9b reveals that there is an interannual modulation in their amplitude: relatively weak signals are detected from 2000 to 2002, in the year between mid 2004 and mid 2005, and in 2007.

4.1. Time Lag Between the Forcing and the Ocean Response

[26] In order to further clarify the relationship between the eddy formation processes and the dipole-structured trade wind forcing, we apply the Ekman pumping model equation (2) to the areas surrounding the Hawaiian Islands. Figure 10 shows the map of the linear correlation coefficient between the observed SSH anomaly data and h'_{EK} interpolated to the Archiving, Validation, and Interpretation of Satellite Oceanographic data altimetry grid points. Here, the correlation is calculated for the period from 1 January 2003 to 4

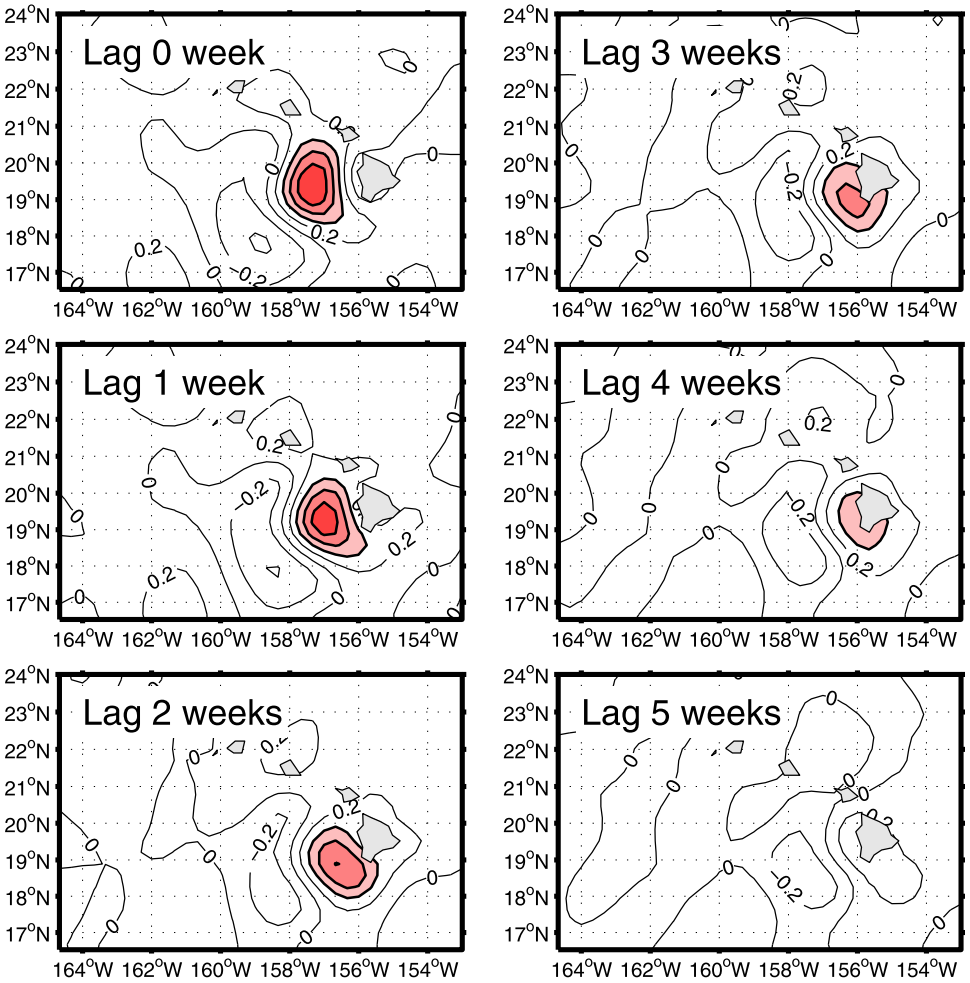

Figure 11. Lagged correlation map between the observed SSH anomalies at the center of Region E (i.e., 19.5°N) and the surrounding grid points. The contour interval is 0.2, and the areas where the correlation coefficient is larger than 0.4 are shown in color.

October 2006, during which the observed 60 day variability is relatively prominent (see Figure 9). The contour in Figure 10 indicates the mean wind forcing distribution (same as Figure 3). One area where the correlation is positive and significant (with the length of the time series at 1370 days, the number of degrees of freedom for the 60 day signals is about 23; in this case, the 90% confidence level corresponds to a correlation coefficient at 0.35) is southwest of the island of Hawaii, where the mean wind stress curl forcing is negative. Although the correlation is also positive to the northwest of Hawaii, where the mean wind stress curl forcing is positive, its magnitude is much smaller. This result implies that it is the anomalous wind stress curl forcing to the southwest of Hawaii that is responsible for initiating the 60 day eddy signals detected in Region E.

[27] To further verify the above suggestion that the SSH anomalies in Region E originate at southwest of the island of Hawaii, we calculate the correlation between the observed SSH anomaly time series (<180 day periods) at the center of Region E and those at surrounding grid points with a lag from 0–5 weeks. Note that the area where the correlation coefficient is larger than 0.4 is given in color in Figure 11. By tracking the high-correlation area, we can see that the SSH anomalies at the center of Region E start from the west of the island of Hawaii with a lag of 2–3 weeks, and they show no clear relation with the SSH anomalies existing farther to the east of the island of Hawaii. To provide a direct comparison, we superimpose in Figure 12a the SSH anomaly time series at 18.6°N, 156.7°W (southwest of island of Hawaii) and at 19.5°N, 157.3°W at the center of Region E. The correspondence between the two time series is visually obvious, and the lagged correlation (Figure 12b), with a maximum coefficient at the 2 week lag, is consistent with the spatial correlation map of Figure 11. The above results confirm that the strong 60 day variability responsible for the enhanced EKE signals in Region E has its origin in the wind-induced SSH anomalies southwest of the island of Hawaii.

4.2. Initial Phases Between the Forcing and the Sea Surface Height Anomaly

[28] In order to obtain an evolving two-dimensional pattern between the wind forcing and phases of the 60 day

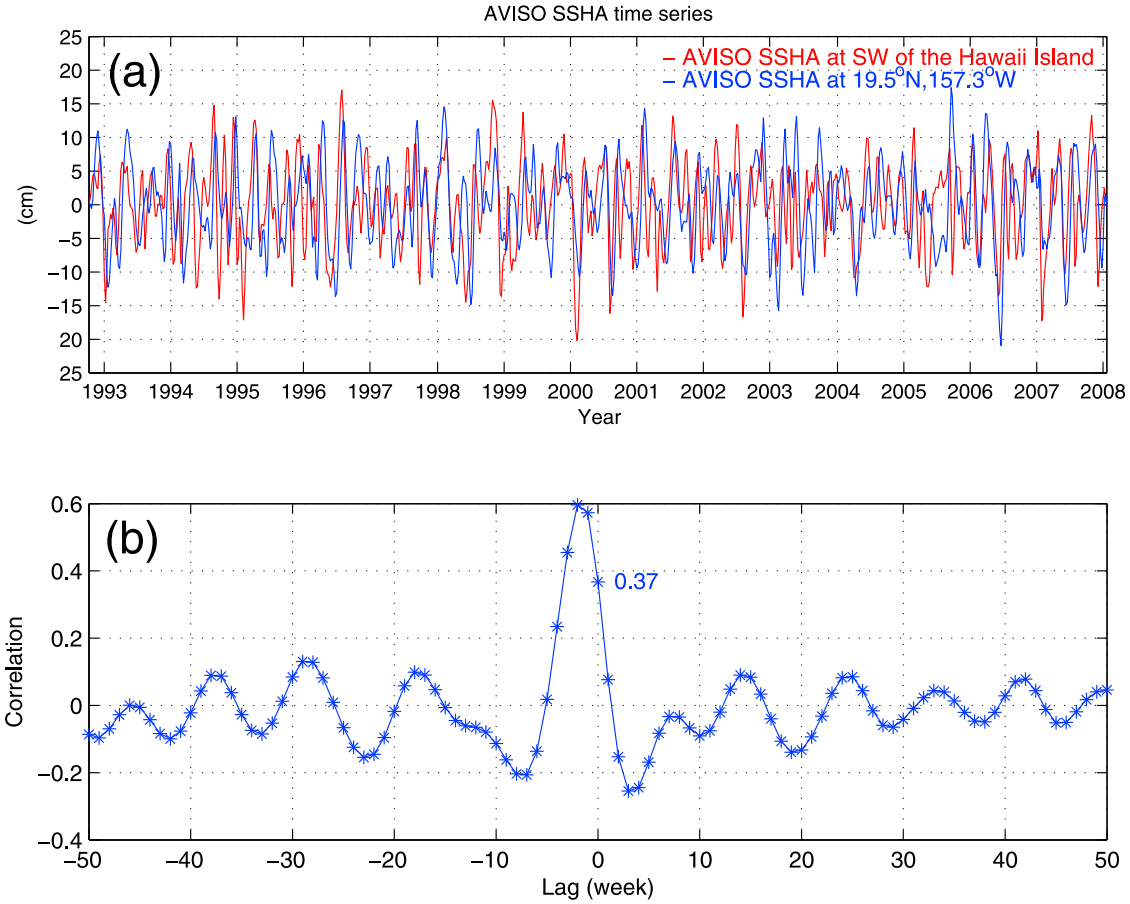

Figure 12. (a) SSH anomaly time series at 19.5°N, 157.3°W (blue curves) and southwest of the island of Hawaii at 18.6°N, 156.7°W (red curves). (b) Lag correlation between the two time series.

variability in the vicinity of the Hawaiian Islands, we conduct a composite analysis based on the observed SSH anomaly data. Figure 13 (left) illustrates the composite SSH anomaly maps, which track the cold-core eddy formation on a weekly basis. Here, the composites are formed from 33 negative SSH anomaly events southwest of the island of Hawaii, whose amplitudes exceed 1.5 times the local SSH standard deviation from 21 July 1999 to 23 January 2008. Prior to the composite, we removed the low-frequency SSH signals with periods >180 days, and "week 0" (Figure 13, bottom left) is defined as when the SSH anomaly southwest of Hawaii exceeds the standard deviation criterion. Figure 13 (right) shows the wind stress curl composites concurrent to the negative SSH composites.

[29] From Figure 13, it is clear that the positive wind stress curl responsible for generating large negative SSH anomalies southwest of Hawaii tends to appear 2 weeks earlier and has maximum amplitude at 1 week earlier. By the time the wind-induced negative SSH anomalies are fully developed at "week 0," the local wind forcing has already weakened. Similar results are also obtained for the positive SSH composites and their connections to the local negative wind stress curl forcing (not shown). Since the large-amplitude, 60 day SSH anomalies take 1–2 weeks to fully grow, it is important to stress that the real-time observed wind stress data could be used for the prediction of the SSH anomalies in the lee of Hawaii.

4.3. Eddy Propagation and Decay Process

[30] To explore how the wind-induced SSH anomalies southwest of island of Hawaii behave after they reach their maximum amplitude, we plot in Figure 14 the negative SSH anomaly composites after they reach maximum amplitudes. The asterisks show the center of the weekly eddy trajectories. Here, the composite maps are presented on a biweekly basis using the same data set as in the previous subsection.

[31] After the SSH anomalies are fully developed, they tend to detach from southwest of the island of Hawaii and travel to the west while gradually decaying in amplitude. This decay reflects the lack of continued wind stress curl forcing to maintain the anomalies' strength against the background dissipation. After 6 weeks or so, the negative SSH anomalies tend to change propagation direction to the northwest. This northwestward drift by the cyclonic eddies is consistent with theories for nonlinear vortices caused by the β effect and self-advection [*Chelton et al.*, 2007]. With the phase speed of the long baroclinic Rossby wave estimated at 7– 8 cm/s at the HLCC, the SSH anomalies are expected to move westward about 5° in 10 weeks. This is comparable to the distance revealed in our composite analysis. After the center of the negative SSH anomalies reaches 160°W, their amplitudes drop further, and there exists a tendency for the site of the SSH anomalies to expand laterally. This decay process further confirms that the wind-

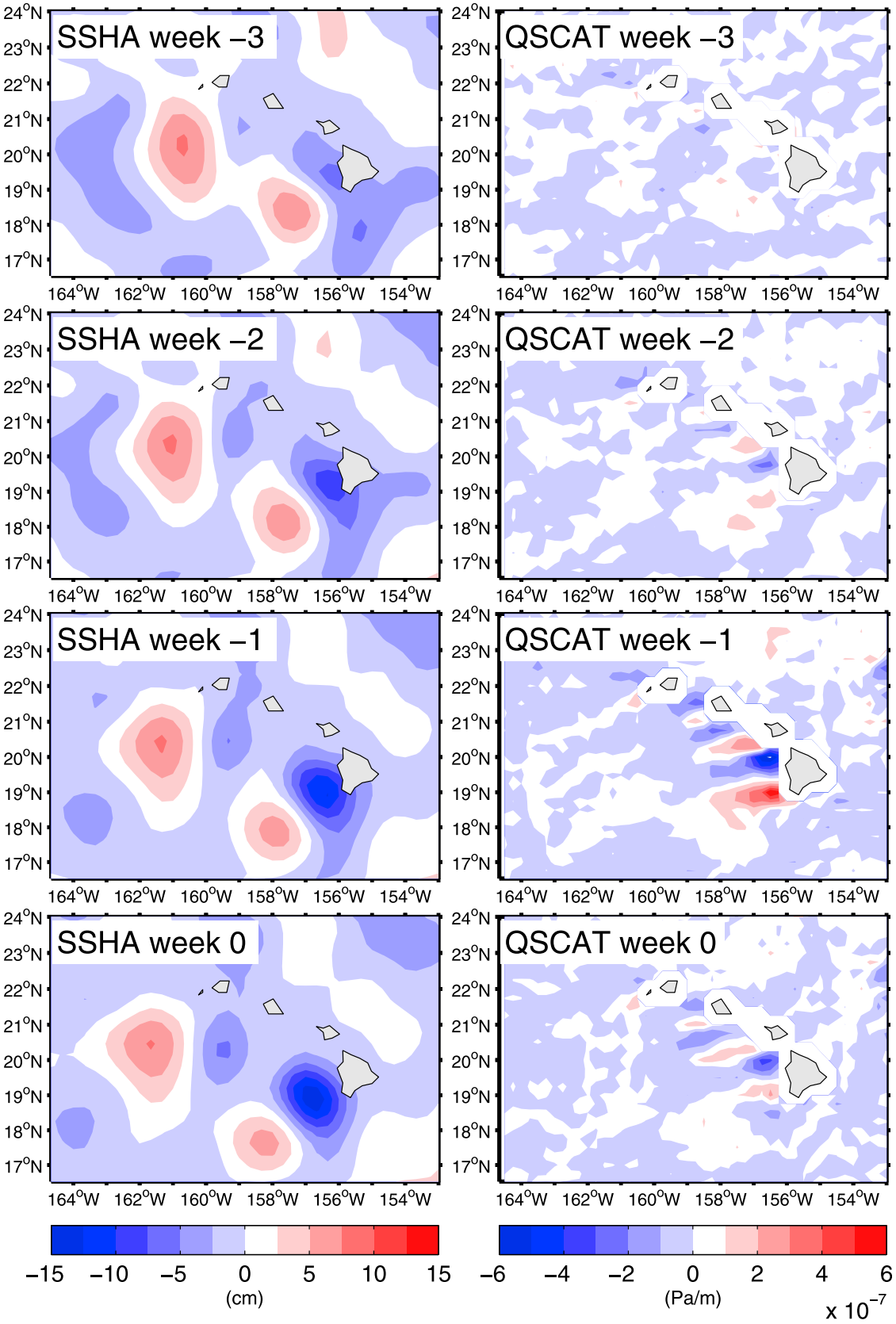

Figure 13. Composite analysis of (left) the observed SSH anomaly and (right) the wind stress curl.

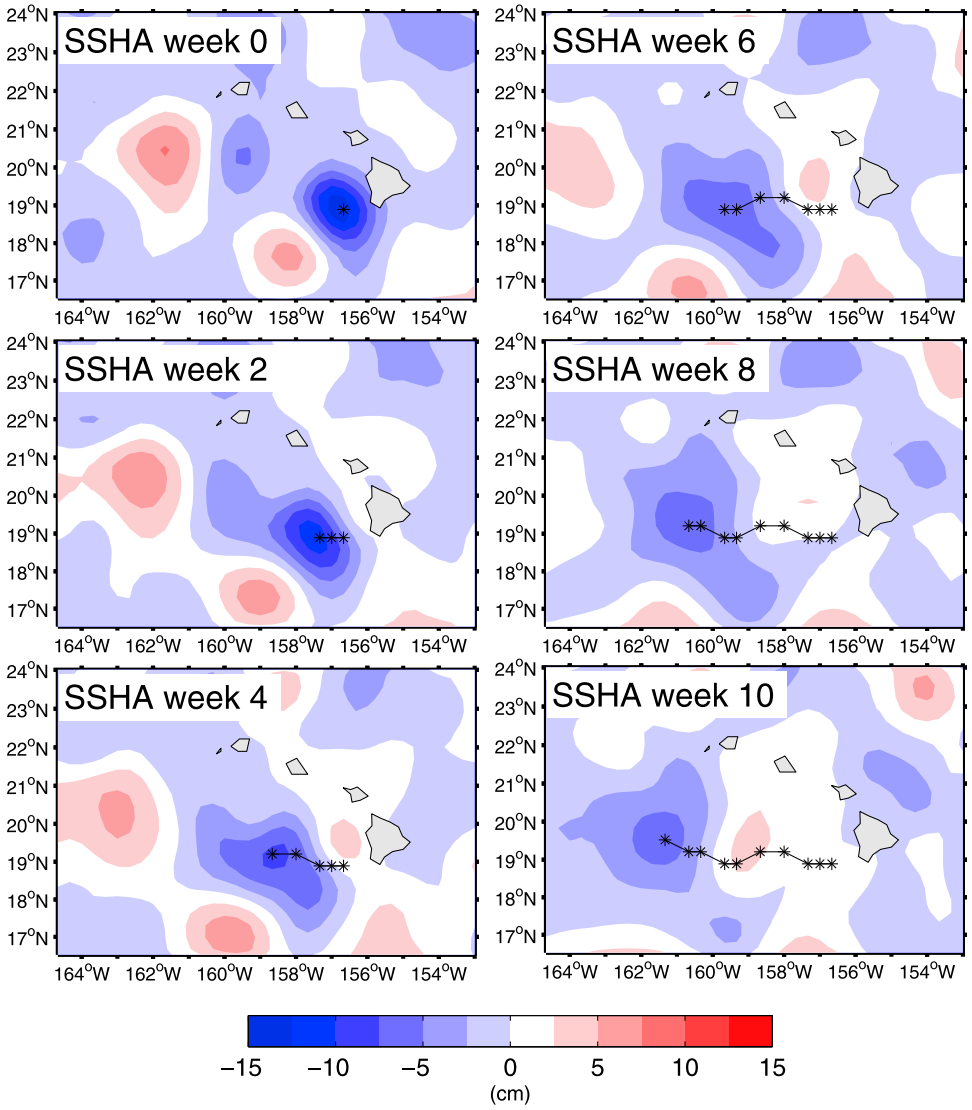

Figure 14. Composite 60 day eddy formation process from week 0 to week 10 after the eddy reaches 1.5 times the standard deviation anomaly at southwest of the island of Hawaii. Asterisks show the center of the eddy for each week.

induced 60 day signals in the lee of the island of Hawaii are not directly connected to the 100 day variability in Region W.

5. Summary and Discussion

[32] By analyzing the weekly altimeter SSH anomaly data accumulated over the last 15 years, we identified two dynamically distinct regions in the lee of the island of Hawaii: a maximum EKE region to the immediate southwest of Hawaii (Region E) and a maximum RMS SSH variability region along 19°N extending westward from ~160°W (Region W). The eddy variability in Region E and Region W has distinguishable time scales at 60 and 100 days, respectively. Reflecting the different governing dynamics in these two regions, the spatial scales of the eddy variability in these two regions are also different. In Region E, the spatial scale of the 60 day variability is relatively small (<200 km) and is governed by the regional wind stress curl anomalies. On the other hand, the 100 day eddy signals in Region W are likely due to the combined barotropic and baroclinic instability of the horizontally and vertically sheared HLCC/NEC system. Their spatial scales are of order 300–400 km and are governed by the propagating baroclinic Rossby waves.

[33] The linear Ekman pumping model was adopted in this study to quantify the 60 day eddy signals in Region E in response to the regional wind stress curl anomalies due to the blocking of the trade wind by the island of Hawaii. We identified the role of the ocean as an integrator that responds more effectively to the lower-frequency synoptic atmospheric forcing than to other, higher-frequency forcing. This is in spite of the fact that the latter forcing has higher variance than that of the 60 day forcing.

[34] In addition to the dynamic analysis based on the Ekman pumping model, this study also used statistical analysis methods to study the formation and evolution of the SSH anomalies. The lagged correlation analysis revealed that the 60 day eddy signals observed in Region E began at

the southwest of the island of Hawaii with a lag of 2 weeks. The composite analysis further revealed that the 60 day signals have short life span and are confined to the lee of the island of Hawaii. This result confirms that the 60 day signals are generated by processes different from those responsible for the 100 day signals in Region W.

[35] Clarifying the cause for the observed 60 day signals has implications for the prediction of mesoscale eddy signals in Region E. Because the 60 day eddies are wind-induced, it is possible to use the real-time, observational wind stress data to predict the eddy development with a lead time of 1–2 weeks. If the cause for the 60 day signals was the NEC's instability, there would be no predictability, as eddy shedding associated with instability of a mean current is intrinsically unpredictable.

[36] We have not addressed the large-scale wind variations in this study. These variations could be important to the interannually varying 60 day signals, which were detected in the satellite altimeter SSH data (see Figure 9b). The large-scale wind variability could change the large-scale mean current systems of the NEC/HLCC, which, in turn, could influence the 60 day eddy signals through changes in regional stratification and dissipative process. Future investigations are needed to unravel the relationship between the interannually varying large-scale wind variability and its influence on the 60 day variability.

[37] **Acknowledgments.** The surface drifter velocity data presented in Figure 1 were generously provided to us by Nikolai Maximenko. Careful comments from Frank Bryan and an anonymous reviewer helped to improve an early version of the manuscript. The altimeter product and surface wind data were provided by the CLS Space Oceanography Division and the Remote Sensing Systems and NASA Ocean Vector Winds Science Team. We acknowledge support from the NOAA through grant NA17RJ1230 to S.Y. and P.H. and from NASA through grant 1207881 to B.Q. This is IPRC publication 651 and SOEST publication 7842.

References

Calil, P. H. R., K. J. Richards, Y. Jia, and R. R. Bidigare (2008), Eddy activity in the lee of the Hawaiian Islands, *Deep Sea Res., Part II*, *55*, 10–13, doi:10.1016/j.dsr2.2008.01.008.

Chelton, D. B., R. A. deSzoeke, M. G. Schlax, K. E. Naggar, and N. Siwertz (1998), Geographical variability of the first baroclinic Rossby radius of deformation, *J. Phys. Oceanogr.*, *28*, 433–460, doi:10.1175/1520-0485(1998)028<0433:GVOTFB>2.0.CO;2.

Chelton, D. B., M. G. Schlax, R. M. Samelson, and R. A. deSzoeke (2007), Global observations of large oceanic eddies, *Geophys. Res. Lett.*, *34*, L15606, doi:10.1029/2007GL030812.

Clarke, A. J. (1998), Inertial wind path and sea surface temperature patterns near the Gulf of Tehuantepec and Gulf of Papagayo, *J. Geophys. Res.*, *93*, 15,494–15,501.

Dickey, T. D., F. Nencioli, V. Kuwahara, C. Leonard, W. Black, R. Bidigare, Y. Rii, and Q. Zhang (2008), Physical and bio-optical observations of oceanic cyclones west of the island of Hawaii, *Deep Sea Res., Part II*, *55*, 1195–1217, doi:10.1016/j.dsr2.2008.01.006.

Firing, E. (1996), Currents observed north of Oahu during the first five years of HOT, *Deep Sea Res., Part II*, *43*, 281–303, doi:10.1016/0967-0645(95)00097-6.

Firing, E., B. Qiu, and W. Miao (1999), Time-dependent island rule and its application to the time-varying north Hawaiian ridge current, *J. Phys. Oceanogr.*, *29*, 2671–2688, doi:10.1175/1520-0485(1999)029<2671:TDIRAI>2.0.CO;2.

Giese, B. S., J. A. Carton, and L. J. Holl (1994), Sea level variability in the eastern tropical Pacific as observed by TOPEX and Tropical Ocean-Global Atmosphere Tropical Atmosphere-Ocean Experiment, *J. Geophys. Res.*, *99*, 24,739–24,748, doi:10.1029/94JC01814.

Hasselmann, K. (1976), Stochastic climate models: Part I. Theory, *Tellus*, *28*(6), 473–485.

Hasunuma, K., and K. Yoshida (1978), Splitting the subtropical gyre in the western North Pacific, *J. Oceanogr. Soc. Jpn.*, *34*, 160–172, doi:10.1007/BF02108654.

Holland, C. L., and G. T. Mitchum (2001), Propagation of Big Island eddies, *J. Geophys. Res.*, *106*, 935–944, doi:10.1029/2000JC000231.

Kobashi, F., and H. Kawamura (2002), Seasonal variation and instability nature of the North Pacific Subtropical Countercurrent and the Hawaiian Lee Countercurrent, *J. Geophys. Res.*, *107*(C11), 3185, doi:10.1029/2001JC001225.

Kuwahara, V., F. Nencioli, T. D. Dickey, Y. Rii, and R. Bidigare (2008), Physical dynamics and biological implications of Cyclone Noah in the lee of Hawaii during E-Flux I, *Deep Sea Res., Part II*, *55*, 1231–1251, doi:10.1016/j.dsr2.2008.01.007.

Lamb, H. (1945), *Hydrodynamics*, 6th ed., Dover, Mineola, N. Y.

Lavín, M. F., J. M. Robles, M. L. Argote, E. D. Barton, R. Smith, J. Brown, M. Kosro, A. Trasviña, H. S. Vélez Muñoz, and J. García (1992), Física del Golfo de Tehuantepec, *Rev. Cienc. Desarrollo*, *18*(103), 97–108.

Lumpkin, D. F. (1998), Eddies and currents in the Hawaiian Island, Ph.D. dissertation, School of Ocean and Earth Sci. and Technol., Univ. of Hawaii, Manoa.

Maximenko, N. A., O. V. Melnichenko, P. P. Niiler, and H. Sasaki (2008), Stationary mesoscale jet-like features in the ocean, *Geophys. Res. Lett.*, *35*, L08603, doi:10.1029/2008GL033267.

McCreary, J. P., Jr., H. S. Lee, and D. B. Enfield (1989), The response of the coastal ocean to strong offshore winds: With application to the gulfs of Tehuantepec and Papagayo, *J. Mar. Res.*, *47*, 81–109, doi:10.1357/002224089785076343.

Mitchum, G. T. (1995), The source of the 90 day oscillations at Wake Island, *J. Geophys. Res.*, *100*, 2459–2475, doi:10.1029/94JC02923.

Müller-Karger, F. E., and C. Fuentes-Yaco (2000), Characteristics of wind-generated rings in the eastern tropical Pacific Ocean, *J. Geophys. Res.*, *105*, 1271–1284, doi:10.1029/1999JC900257.

Nencioli, F., V. Kuwahara, T. D. Dickey, Y. Rii, and R. Bidigare (2008), Physical dynamics and biological implications of a mesoscale eddy in lee of Hawaii: Cyclone Opal observations during E-Flux III, *Deep Sea Res., Part II*, *55*, 1252–1274, doi:10.1016/j.dsr2.2008.02.003.

Qiu, B. (1999), Seasonal eddy field modulation of the North Pacific Subtropical Countercurrent: TOPEX/Poseidon observations and theory, *J. Phys. Oceanogr.*, *29*, 2471–2486, doi:10.1175/1520-0485(1999)029<2471:SEFMOT>2.0.CO;2.

Qiu, B. (2002), Large-scale variability in the midlatitude subtropical and subpolar North Pacific Ocean: Observations and causes, *J. Phys. Oceanogr.*, *32*, 353–375, doi:10.1175/1520-0485(2002)032<0353:LSVITM>2.0.CO;2.

Qiu, B., and T. S. Durland (2002), Interaction between an island and the ventilated thermocline: Implications for the Hawaiian Lee Countercurrent, *J. Phys. Oceanogr.*, *32*, 3408–3426, doi:10.1175/1520-0485(2002)032<3408:IBAIAT>2.0.CO;2.

Qiu, B., D. A. Koh, C. Lumpkin, and P. Flament (1997), Existence and formation mechanism of the North Hawaiian Ridge Current, *J. Phys. Oceanogr.*, *27*, 431–444, doi:10.1175/1520-0485(1997)027<0431:EAFMOT>2.0.CO;2.

Sakamoto, T. T., A. Sumi, S. Emori, T. Nishimura, H. Hasumi, T. Suzuki, and M. Kimoto (2004), Far-reaching effects of the Hawaiian Islands in the CCSR/NIES/FRCGC high-resolution climate model, *Geophys. Res. Lett.*, *31*, L17212, doi:10.1029/2004GL020907.

Sasaki, N., and M. Nonaka (2006), Far-reaching Hawaiian Lee Countercurrent driven by wind-stress curl induced by warm SST band along the current, *Geophys. Res. Lett.*, *33*, L13602, doi:10.1029/2006GL026540.

Trasviña, A., E. D. Barton, J. Brown, H. S. Velez, P. M. Kosro, and R. L. Smith (1995), Offshore wind forcing in the Gulf of Tehuantepec, Mexico: The asymmetric circulation, *J. Geophys. Res.*, *100*, 20,649–20,663, doi:10.1029/95JC01283.

Uda, M., and K. Hasunuma (1969), The Eastward Subtropical Countercurrent in the western North Pacific Ocean, *J. Oceanogr. Soc. Jpn.*, *25*, 201–210.

Xie, S. P., W. T. Liu, and M. Nonaka (2001), Far-reaching effects of the Hawaiian Islands on the Pacific Ocean-atmosphere system, *Science*, *292*, 2057–2069, doi:10.1126/science.1059781.

Zamudio, L., H. E. Hurlburt, E. J. Metzger, S. L. Morey, J. J. O'Brien, C. Tilburg, and J. Zavala-Hidalgo (2006), Interannual variability of Tehuantepec eddies, *J. Geophys. Res.*, *111*, C05001, doi:10.1029/2005JC003182.

P. Hacker and S. Yoshida, International Pacific Research Center, University of Hawai'i at Mānoa, 1680 East-West Rd., POST Bldg. 401, Honolulu, HI 96822, USA. (sachikoy@hawaii.edu)

B. Qiu, Department of Oceanography, University of Hawai'i at Mānoa, 1680 East-West Rd., Honolulu, HI 96822, USA.